TECHNICAL REPORT CR-RD-PR-88-1

PRELIMINARY INVESTIGATION OF FLOW MODELING DURING SOLID PROPELLANT PROCESSING

H. M. Dornanus
W. T. Sha
Analytical Thermal Hydraulic Research Program
Argonne National Laboratory
Argonne, Illinois 60439

and

S. L. Soo
Department of Mechanical and Industrial Engineering
University of Illinois-Urbana
Urbana, Illinois 61801

Prepared for:

Propulsion Directorate
Research, Development, and Engineering Center

FEBRUARY 1988

U.S. ARMY MISSILE COMMAND
Redstone Arsenal, Alabama 35898-5000

UNCLASSIFIED
SECURITY CLASSIFICATION OF THIS PAGE

AD-A196 168

REPORT DOCUMENTATION PAGE

Form Approved
OMB No 0704-0188
Exp Date Jun 30, 1986

1a REPORT SECURITY CLASSIFICATION UNCLASSIFIED	1b. RESTRICTIVE MARKINGS None
2a. SECURITY CLASSIFICATION AUTHORITY	3. DISTRIBUTION/AVAILABILITY OF REPORT Approved for public release, distribution is unlimited.
2b. DECLASSIFICATION/DOWNGRADING SCHEDULE	
4. PERFORMING ORGANIZATION REPORT NUMBER(S)	5. MONITORING ORGANIZATION REPORT NUMBER(S) CR-RD-PR-88-1
6a. NAME OF PERFORMING ORGANIZATION Argonne National Laboratory Components Technology Div 6b. OFFICE SYMBOL (If applicable)	7a. NAME OF MONITORING ORGANIZATION U.S. Army Missile Command Propulsion Directorate
6c. ADDRESS (City, State, and ZIP Code) 9700 South Cass Avenue Argonne, IL 60439	7b. ADDRESS (City, State, and ZIP Code) AMSMI-RD-PR-E Redstone Arsenal, AL 35898-5249
8a. NAME OF FUNDING/SPONSORING ORGANIZATION US Army Missile Command 8b. OFFICE SYMBOL (If applicable) AMSMI-RD-PR	9. PROCUREMENT INSTRUMENT IDENTIFICATION NUMBER Contract No. W-31-109-ENG-38
8c. ADDRESS (City, State, and ZIP Code) Redstone Arsenal, AL 35898	10. SOURCE OF FUNDING NUMBERS PROGRAM ELEMENT NO. 61101A; PROJECT NO. 1L161101A91A; TASK NO.; WORK UNIT ACCESSION NO.

11. TITLE (Include Security Classification)

Preliminary Investigation of Flow Modeling During Solid Propellant Processing

12. PERSONAL AUTHOR(S)

H. M. Domanus, W. T. Sha, S. L. Soo

13a. TYPE OF REPORT	13b. TIME COVERED	14. DATE OF REPORT (Year, Month, Day)	15. PAGE COUNT
Interim	FROM 5/86 TO 9/87	1988/Feb/19	36

16. SUPPLEMENTARY NOTATION

17. COSATI CODES			18. SUBJECT TERMS (Continue on reverse if necessary and identify by block number)
FIELD	GROUP	SUB-GROUP	Propellant Processing Flow Modeling Liquid/Solid Flows
21	08		

19. ABSTRACT (Continue on reverse if necessary and identify by block number)

The results of preliminary modeling of a solid propellant flow as would occur during propellant casting is presented. Both single and multiple velocity field models were investigated. Results with the single velocity field model produced solid particle segregation that was in qualitative agreement with experience. It is the objective of this work to understand and ultimately predict the composition gradients that result during solid propellant processing.

20. DISTRIBUTION/AVAILABILITY OF ABSTRACT ☒ UNCLASSIFIED/UNLIMITED ☐ SAME AS RPT. ☐ DTIC USERS	21. ABSTRACT SECURITY CLASSIFICATION UNCLASSIFIED
22a. NAME OF RESPONSIBLE INDIVIDUAL A. R. Maykut	22b TELEPHONE (Include Area Code) (205)-876-4656 22c. OFFICE SYMBOL AMSMI-RD-PR

DD FORM 1473, 84 MAR

83 APR edition may be used until exhausted.
All other editions are obsolete.

SECURITY CLASSIFICATION OF THIS PAGE

UNCLASSIFIED

TECHNICAL REPORT CR-RD-PR-88-1

PRELIMINARY INVESTIGATION OF FLOW MODELING DURING SOLID PROPELLANT PROCESSING

by

H. M. Domanus
W. T. Sha
Analytical Thermal Hydraulic Research Program
Materials and Components Technology Division
Argonne National Laboratory
9700 South Cass Avenue
Argonne, Illinois 60439

and

S. L. Soo
Department of Mechanical and Industrial Engineering
University of Illinois-Urbana
Urbana, Illinois 61801

Prepared for

Propulsion Directorate
Research, Development, and Engineering Center

FEBRUARY 1988

CONTENTS

1. OBJECTIVE

The objective of the proposed work is to develop a computer model capable of predicting the distribution of solid particle constituents during the processing of solid propellants.

2. INTRODUCTION

In order to control the propellant burning rate and, hence, the propulsive performance of a solid rocket motor, it is essential to create a desired particle distribution throughout a solid propellant. It is therefore desirable to determine, via computation, the distribution of particulates during casting of solid rocket fuel. The present program, fundamental in nature, is geared toward initiating, understanding, and modeling the mechanisms that control the distribution of solid particle constituents during the processing of a solid propellant.

The propellant casting can be considered as a multiphase flow process with a dense suspension fluid in creeping motion. In such a case, the shear resistance (shear lift phenomenon), relaxation phenomenon due to particle-particle interaction, particle-fluid interaction, and particle-wall interaction predominate even though the fluid phase (binders) may be serving the main function of transporting. Even if we start with a uniform mix of particles of various sizes, non-uniformity may result from:

(1) particle-fluid interactions alone - small particles due to shear lift force tend to move away from the wall faster than large particles.

(2) particle-particle interactions alone - small particles tend to act as a fluid, exerting a shear lift force on the large particles. The large particles tend to move away from the wall faster than the small particles.

(3) the boundary condition at the wall where the fluid velocity must be zero, but the particle velocity may have a finite value (slip motion). Thus, particles tend to migrate toward the center of the passage or away from the wall.

These expected facts[1] are in agreement with observation by Bradfield[2] of WRE (Weapons Research Establishment).

In treating the present problem of transient flow with solids of various particle sizes in a liquid suspension, we need to consider:

(1) shear lift phenomenon,

(2) particle-particle interaction,

(3) particle-fluid interactions, and

(4) particle-wall interactions.

The shear lift phenomenon of solid particles in a fluid was formulated by Saffman[3], studied experimentally by Segré and Silberberg[4], and correlated by Soo[5], including the resultant concentration in steady or depositing flow[6]. The effect of particle diffusivity was found to be important. Segré and Silberberg[4] particularly identified that in laminar pipe flow of a suspension of neutral buoyancy, the maximum concentration of particles tends to occur at 2/3 radius from the pipe axis, that is, toward the wall, than toward the center. Many of these basic relations concerning the distribution of particulates in a fluid need to be synthesized and formulated for the present system.

It should be noted that very little work has been done, both experimentally and theoretically, on dense suspension systems.

3. MATHEMATICAL MODELING

3.1 Multiple Velocity Field Model or Multifluid Model

Use of a multiple velocity field model calls for a set of formulations including continuity and momentum equations of phases, or in the present case,

components. The continuity equations are

$$\frac{\partial \theta_1 \rho_1}{\partial t} + \nabla \cdot (\theta_1 \rho_1 \underline{U}_1) = 0 \tag{1}$$

$$\frac{\partial \theta_2 \rho_2}{\partial t} + \nabla \cdot (\theta_2 \rho_2 \underline{U}_2) = 0 \tag{2}$$

$$\frac{\partial \theta_3 \rho_3}{\partial t} + \nabla \cdot (\theta_3 \rho_3 \underline{U}_3) = 0 \tag{3}$$

where θ_1, ρ_1, $\underline{U}_1$ refer to the volume fraction, the material density, and the velocity of the binder; subscripts 2 refer to the aluminum powder and 3 refers to the ammonium perchlorate powder. For the example of $\theta_1 = 0.2352$, $\theta_2 = 0.1269$, and $\theta_3 = 0.6379$, noting that $\theta_1 + \theta_2 + \theta_3 = 1$. The momentum equations are

$$\frac{\partial \theta_1 \rho_1 \underline{U}_1}{\partial t} + \nabla \cdot (\theta_1 \rho_1 \underline{U}_1 \underline{U}_1) = -\theta_1 \nabla P + \nabla \cdot \underline{\tau}_{1m} + \theta_1 \rho_1 \underline{f}_1 - K_{12}(\underline{U}_1 - \underline{U}_2) - K_{13}(\underline{U}_1 - \underline{U}_3) \tag{4}$$

$$\frac{\partial \theta_2 \rho_2 \underline{U}_2}{\partial t} + \nabla \cdot (\theta_2 \rho_2 \underline{U}_2 \underline{U}_2) = -\theta_2 \nabla P + \nabla \cdot \underline{\tau}_{2m} + \theta_2 \rho_2 \underline{f}_2 - K_{21}(\underline{U}_2 - \underline{U}_1) - K_{23}(\underline{U}_2 - \underline{U}_3) \tag{5}$$

$$\frac{\partial \theta_3 \rho_3 \underline{U}_3}{\partial t} + \nabla \cdot (\theta_3 \rho_3 \underline{U}_3 \underline{U}_3) = -\theta_3 \nabla P + \nabla \cdot \underline{\tau}_{3m} + \theta_3 \rho_3 \underline{f}_3 - K_{31}(\underline{U}_3 - \underline{U}_1) - K_{32}(\underline{U}_3 - \underline{U}_2) \tag{6}$$

where P is the pressure, τ_{1m} is the shear stress of component 1 in the mixture, $\underline{f}_1$ is the field force per unit mass on component 1 and may include that due to the shear lift effect*. K_{12} is the interfacial momentum transfer coefficient including drag between phase 2 and phase 1, etc., where

*The magnitude of shear lift here is seen not to be influenced by the rotation of the particles[3].

$$K_{12} = \theta_1 \rho_1 F_{12}, \text{ etc.}$$

F_{12} is the inverse relaxation time for momentum transfer from phase 2 to phase 1, etc., and

$$\theta_1 \rho_1 F_{12} = \theta_2 \rho_2 F_{21} \qquad \text{or} \qquad K_{12} = K_{21}$$

etc. from action and reaction. With correct boundary conditions, Eqs. 1 to 6 are solved for an isothermal system to determine the volume fraction and velocity distribution of phases. Transport properties are needed to determine τ_{1m} etc. and F_{12} etc. F_{12}, F_{21}, F_{13}, and F_{31} arise from fluid-particle interaction. F_{23} or F_{32} arises from particle-particle interaction. These quantities depend on the properties of materials and operating conditions; non-Newtonian behaviors are expected for the present system.

For given initial conditions, pertinent boundary conditions for the above equation for flow through a pipe of radius R include

$$r = R, \qquad U_{1z} = 0$$

$$U_{2z} = - L_{21} \left. \frac{\partial U_{2z}}{\partial r} \right|_R$$

$$U_{3z} = - L_{31} \left. \frac{\partial U_{3z}}{\partial r} \right|_R$$

for the axial velocities, where L_{21} is the interaction length of particle to fluid, leading to slip motion and $L_{21} = \left\langle (\Delta u)_{21}^2 \right\rangle^{1/2} / F_{21}$ where $\left\langle \Delta u_{21}^2 \right\rangle^{1/2}$ is the relative intensity of motion of phase 2 in 1, and F_{21} can be large for small particles in a viscous fluid. A limiting case will be

$$\partial U_{2z}/\partial r = \partial U_{3z}/\partial r = 0.$$

Since the particulate material finally set in their place by solidification rather than by deposition, the boundary condition for the volume fraction of

particles at the wall is given by [6] (k = 2, 3)

$$D_{km} \left.\frac{\partial \theta_k}{\partial r}\right|_R = \theta_k f_k / F_{k1}$$

While τ_{1m} is defined according to the multiphase formulation, its determination for the present system is complicated because of a dense suspension. Based on the theory of dense suspensions[7], τ_{1m} is expected to be greater than τ_1 (pure binder). In general τ_m of the mixture is strongly influenced by the perchlorate powder (63% by volume). Unlike the case of a dilute suspension, τ_{1m}, τ_{2m}, τ_{3m} are not readily determined at this time. (In the case of dilute suspensions of 2 and 3, $\tau_{1m} \sim \tau_1$, $\tau_{2m} = D_{2m}\theta_2\rho_2$, $\tau_{3m} = D_{3m}\theta_3\rho_3$; D_{2m} is the diffusivity of particles 2 in the mixture. Likewise, D_{3m} is the diffusivity of particles 3 in the mixture.) In the present case, it suffices to say that $\tau_{2m} \equiv \mu_{2m}\underline{\Delta}_2$, where μ_{2m} is the viscosity of phase 2 in the mixture, $\underline{\Delta}_2$ is the deformation tensor of the motion of phase 2, and μ_{2m} is related to D_{2m} according to the relation of a dense suspension[7].

Computations based on the multifluid model calls for simultaneous solution of Eqs. 1 to 6 with pertinent boundary conditions and accurate transport properties F_{21}, F_{31}, F_{32} and μ_{1m}, μ_{2m}, and μ_{3m}. The latter are not readily computed or measured; often the best we can manage is the viscosity of the mixture. The closeness, though different, of the phase velocities also suggests that the mixture velocity may be sufficiently representative. Thus, it leads us to use the relatively simple single velocity field model as described in the following section.

3.2 Single Velocity Field Model

Summing Eqs. 4, 5, and 6 gives the momentum equation of the mixture as

$$\frac{\partial \rho_m \underline{U}_m}{\partial t} + \nabla \cdot \left(\rho_m \underline{U}_m \underline{U}_m\right) + \nabla \cdot \sum_{1,2,3} \theta_k \rho_k \left(\underline{U}_k - \underline{U}_m\right)\left(\underline{U}_k - \underline{U}_m\right)$$

$$= - \nabla P + \nabla \cdot \underline{\tau}_m + \rho_m \underline{f}_m \tag{7}$$

$\underline{\tau}_m = \mu_m \underline{A}$ while internal action and reaction for momentum transfer cancel each other. The mixture density and velocity are defined by

$$\rho_m = \sum_{1,2,3} \theta_k \rho_k$$

and

$$\rho_m \underline{U}_m = \sum_{1,2,3} \theta_k \rho_k \underline{U}_k \tag{8}$$

while the field force is given by

$$\rho_m \underline{f}_m = \sum_{1,2,3} \theta_k \rho_k \underline{f}_k$$

for k = 1, 2, 3 as in Section 3.1. For a dense mixture, the velocity difference $(\underline{U}_k - \underline{U}_m)$ is small and the third term on the left side of Eq. 7 can be neglected.

Equations. 2 and 3 can be modified by considering the continuity equation of the mixture obtained from summing Eqs. 1, 2, and 3, or

$$\frac{\partial \rho_m}{\partial t} + \nabla \cdot \rho_m \underline{U}_m = 0 . \tag{9}$$

The continuity equation of species k (k = 2, 3) can be rewritten as

$$\frac{\partial \rho_k \theta_k}{\partial t} + \nabla \cdot (\rho_k \theta_k \underline{U}_m) = \nabla \cdot \rho_k \theta_k (\underline{U}_m - \underline{U}_k). \tag{10}$$

Since $\rho_k \theta_k (\underline{U}_k - \underline{U}_m) = \underline{J}_k$, the general flux of phase k, we have

$$\frac{\partial \rho_k \theta_k}{\partial t} + \nabla \cdot (\rho_k \theta_k \underline{U}_m) = - \nabla \cdot \underline{J}_k . \tag{11}$$

or

$$\frac{\partial \rho_k \theta_k}{\partial t} + \underline{U}_m \cdot \nabla \rho_k \theta_k = - \rho_k \theta_k \nabla \cdot \underline{U}_m - \nabla \cdot \underline{J}_k \equiv \frac{d \rho_k \theta_k}{d t_m} \tag{12}$$

In terms of mass fraction $c_k = \theta_k \rho_k / \rho_m$, Eq. 11 becomes

$$\frac{\partial \rho_m c_k}{\partial t} + \nabla \cdot \left(c_k \rho_m \underline{U}_m \right) = - \nabla \cdot \underline{J}_k \ . \tag{13}$$

Subtracting the product of c_k and Eq. 9 from Eq. 13, and rearranging, we get

$$\rho_m \frac{\partial c_k}{\partial t} + \rho_m \underline{U}_m \cdot \nabla c_k = - \nabla \cdot \underline{J}_k \tag{14}$$

or

$$\rho_m \frac{d c_k}{d t_m} = - \nabla \cdot J_k \ . \tag{15}$$

For nearly constant ρ_m, the component continuity equation takes the form

$$\frac{d \rho_k \theta_k}{d t_m} = \frac{\partial \rho_k \theta_k}{\partial t} + \underline{U}_m \cdot \nabla \left(\rho_k \theta_k \right) = - \nabla \cdot \underline{J}_k \ . \tag{16}$$

Either Eqs. 5 or 6, neglecting inertial forces, pressure gradient, and assuming equal particle velocities and binder velocity approximately equal to the mixture velocity, gives

$$\underline{J}_k = \frac{\theta_k \rho_k \underline{f}_k}{F_{kl}} + \nabla \cdot \left(\frac{\mu_{km}}{F_{kl}} \nabla \underline{U}_k \right)$$

$$\simeq \frac{\theta_k \rho_k \underline{f}_k}{F_{kl}} - D_{km} \nabla \left(\rho_k \theta_k \right) \tag{17}$$

for drift by field forces and diffusion by concentration gradient. This is because shear resistance in a suspension arises from resistance to transport of momentum by diffusion. The kinematic viscosity and diffusivity D_{km}, are related by

$$\frac{\mu_{km}}{F_{kl}} \nabla \underline{U}_k \simeq \frac{\theta_k \rho_k}{F_{kl}} \nu_{km} \nabla \underline{U}_k \simeq - \rho_k \theta_k D_{km} \tag{18}$$

with the correspondence of $\left(\nu_{km} / F_{kl} \right) \nabla \underline{U}_k \sim -D_{km}$. This correspondence serves to explain the relation between the diffusion model and the multifluid model. It is noted that the diffusion flux is usually derived in a different manner[8]. Equation 16 now reduces for nearly constant ρ_m to

$$\frac{\partial \rho_k \theta_k}{\partial t} + \underline{U}_m \cdot \nabla (\rho_k \theta_k) = \nabla \cdot [D_{km} \nabla (\theta_k \rho_k) - \underline{f}_k \theta_k \rho_k / F_{k1}] \qquad (19)$$

which is the diffusion equation.

The diffusion equation renders the continuity equation of phase k independent of its momentum equation. However, once θ_k is determined, $\underline{U}_k$ can still be calculated from its momentum equation if it is needed. Often a knowledge of the distribution of θ_k is sufficient. Equations 7, 9, and 19 (k = 2, 3) can be solved for P, θ_1, θ_2, θ_3 and $\underline{U}_m$ for the following boundary conditions:

$$r = R. \qquad \underline{U}_m = 0$$

$$- D_{km} \left. \frac{\partial \rho_k \theta_k}{\partial r} \right|_R = - \rho_k \theta_k \frac{f_k}{F_{k1}}$$

for given initial conditions.

It is recognized that F_{21}, F_{31}, F_{32}, D_{km} and μ_m still have to be determined experimentally for accurate prediction.

4. EXPLORATORY CALCULATIONS

In the process of forming a solid propellant motor, several different particulate materials are mixed together with a polymer binder. The batch is mixed until the mixture becomes uniform and homogeneous. The homogeneous mixture is then passed through a network of pipes and ducts to a mold. As the mixture flows, the components of the mixture begin to displace relative to one another by shear motion. This gives rise to non-uniform propellant properties in the mold and hence the final cured motor.

The ability to calculate partial component separation from a homogeneous mixture is a crucial feature which must be present in the mathematical model. In order to investigate and demonstrate that the proposed mathematical model is capable of simulating this separation phenomena, some exploratory calcula-

tions were made for representative situations. The numerical results presented here were obtained with the COMMIX code[9,10], which was modified to carry out these calculations.

4.1 Numerical Model

Flow into a 6.35E-3 m (0.25 in) gap between two parallel plates and into an annulus is considered. A two-velocity field model is used to describe the flow and component distributions. (Component #1 represents the polymer binder and component #2 represents the particles. The governing equations are discretized by the finite volume technique. The two-dimensional computational domain is partitioned into 8 equal partitions across the gap and 20 along the flow direction. The overall length modeled (0.0254 m) was long enough so that the flow would become fully developed. At the entrance, the mixture is assumed to be homogeneous and have a uniform velocity of 0.01 m/s. The binder (component #1) is assumed to stick to the wall $\left(v_1|_w = 0\right)$, while the particles (component #2) are assumed to have a free slip boundary condition $\left(\left.\frac{\partial v_2}{\partial x}\right|_w\right) = 0$.

A semi-implicit time-marching algorithm was used to solve the system of equations. By marching in time until all quantities (velocity components and volume fraction) converged to one part in 100,000, a steady-state solution was reached.

4.2 Flow Between Parallel Plates

The first problem considered is flow between two parallel plates separated by 6.35E-3 m (0.25 in). A homogeneous 50-50 mixture (by volume) enters the gap uniformly with a velocity of 0.01 m/s. Other characteristics are shown in Table 1. By the time the flow reaches the exit, a fully developed situation exists.

Figure 1 shows the fully developed velocity profiles for the binder (v_1) and the particles (v_2). The differences in the velocity distribution must be

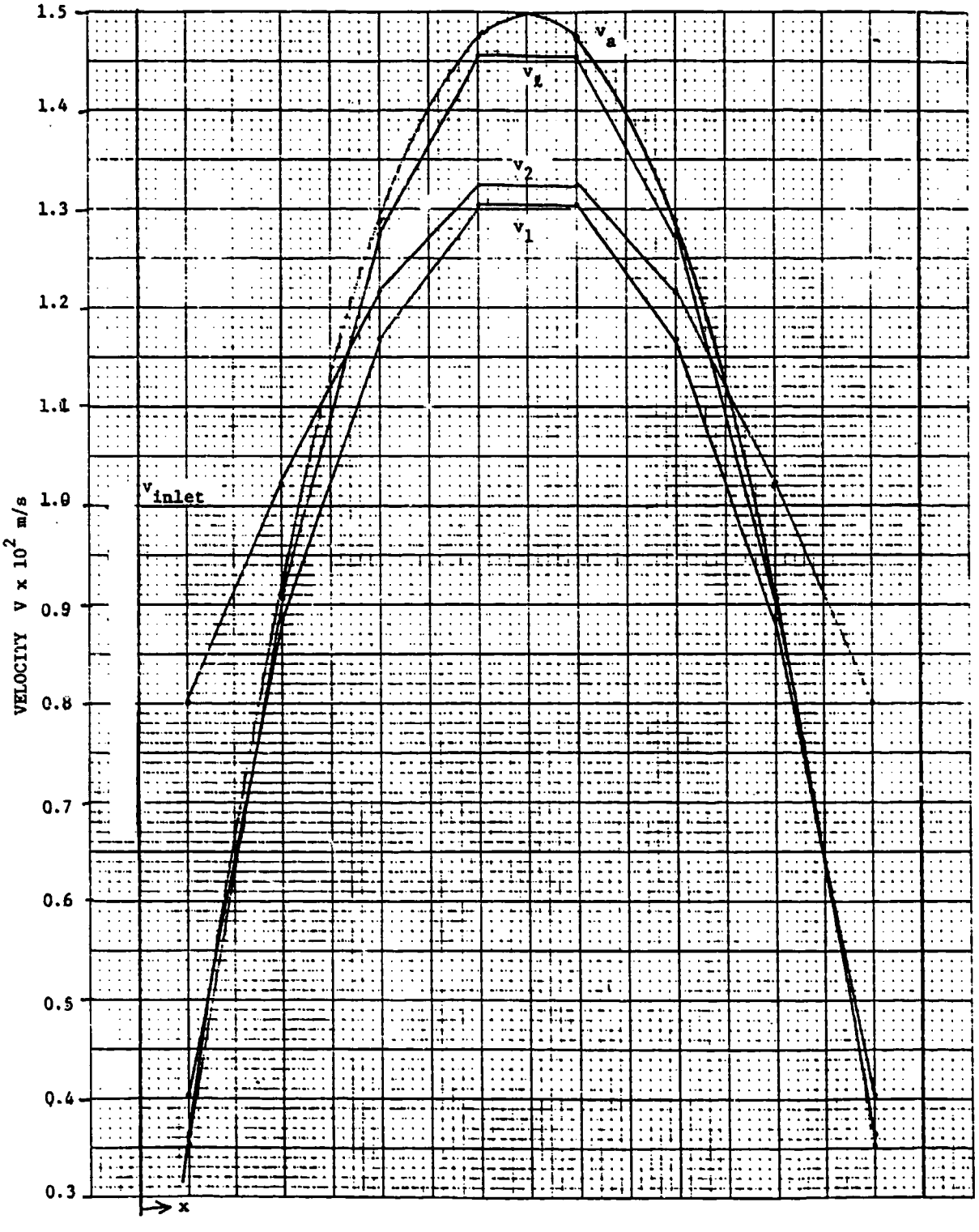

Fig. 1. Fully Developed Flow Between Parallel Plates

TABLE 1. Flow Between Parallel Plates

Gap	6.35E-3 m (0.25 in)
Inlet velocity $v_1 = v_2$	0.01 m/s
Inlet θ_1 (binder)	0.5
θ_2 (particles)	0.5
$\mu_1 = \mu_2$	200 Pa-s
$\rho_1 = \rho_2$	1000 kg/m^3
K_{12}	1.0E8 Pa-s/m^2
Re	3.175E-4

entirely due to the different boundary conditions imposed on the 2 components because the material properties used are the same. This was verified by running a problem where both components had no slip boundaries and this yielded the fully developed velocity profile v_ℓ shown in Fig. 1 for both components. For reference, the well known parabolic velocity profile is also shown and labeled v_a in Fig. 1. Note that the velocity distributions of both the binder and the particles are flatter than the reference case. The particle velocity is consistently higher than the binder velocity throughout the cross-section.

Figure 2 shows the volume fraction distribution of binder (θ_1) and particles (θ_2). It is readily apparent that a partial separation of components has occurred. The particles have a relative maximum concentration in the center of the gap while the binder is more concentrated near the wall.

It is worth noting that this separation phenomena is due entirely to the difference in velocity boundary conditions at the wall for the two components.

4.3 Annular Flow

The second problem considered is two-dimensional axisymmetric flow between two concentric cylindrical surfaces forming an annular region. The problem characteristics are summarized in Table 2. The inner radius is

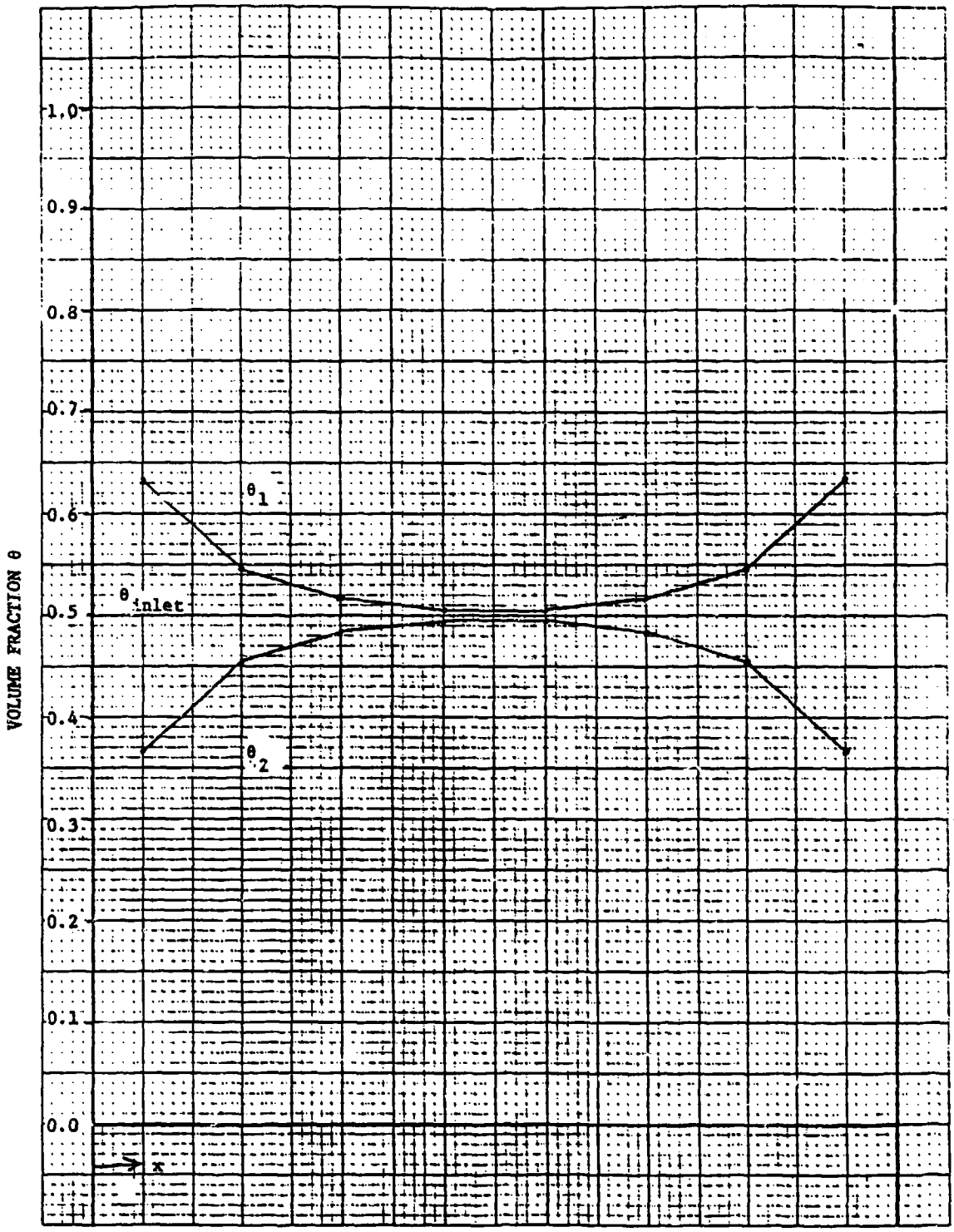

Fig. 2. Fully Developed Volume Fraction Distribution for Flow Between Parallel Pletes

TABLE 2. Flow Into Annulus

R_{in}	0.01905 m (0.75 in)
R_{out}	0.0254 m (1.0 in)
Gap	6.35E-3 m (0.25 in)
Inlet velocity $v_1 = v_2$	0.01 m/s
θ_1 (binder)	0.2242
θ_2 (particles)	0.7758
$\mu_1 = \mu_2$	200 Pa-s
ρ_1 (binder)	920 kg/m^3
ρ_2 (particles)	1950 kg/m^3
K_{12}	1.0E8 Pa-s/m^2

0.01905 m (0.75 in) and the outer radius is 0.0254 (1.0 in). This results in a 6.35E-3 m (0.25 in) annular gap. Here, we have used a homogeneous mixture with a higher particle volume fraction (.77) and a material density difference between the binder (920 kg/m^3) and particles (1950 kg/m^3).

Figure 3 shows the fully developed velocity profiles. The velocity distribution when both components have no slip boundary conditions is labeled v_ℓ. This solution is similar to the parallel plates solution except the central peak velocity occurs nearer the inner surface. The particle velocity (v_2) is consistently higher than the binder velocity (v_1) throughout the cross-section. Due to the higher particle concentration and material density, the velocity profiles are flatter and maximum velocities less than the corresponding results for the parallel plates.

The volume fraction distributions are shown in Fig. 4. The particle volume fractions (θ_2) show the highest value near the middle and lower near

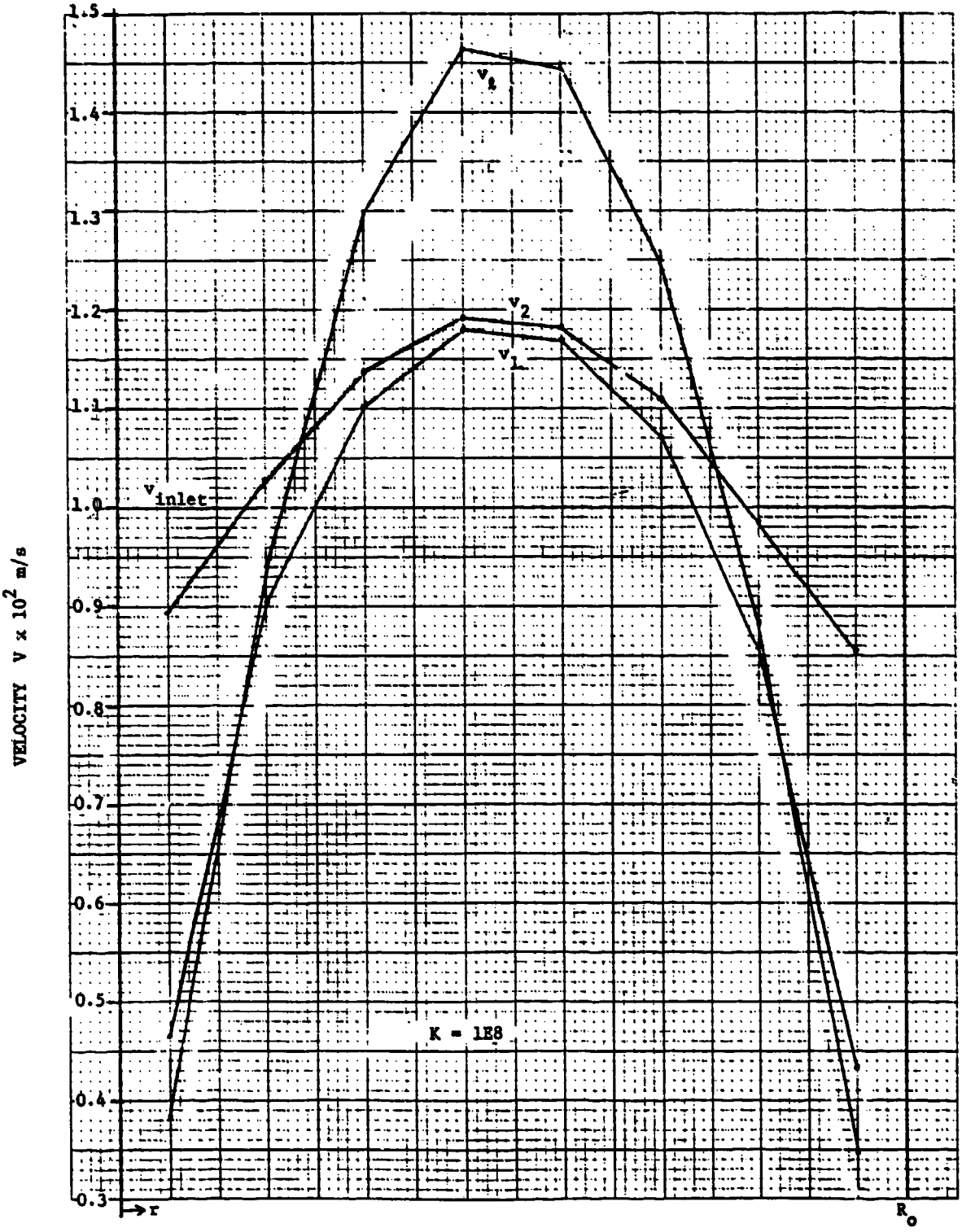

Fig. 3. Velocity Distribution in Fully Developed Annular Flow

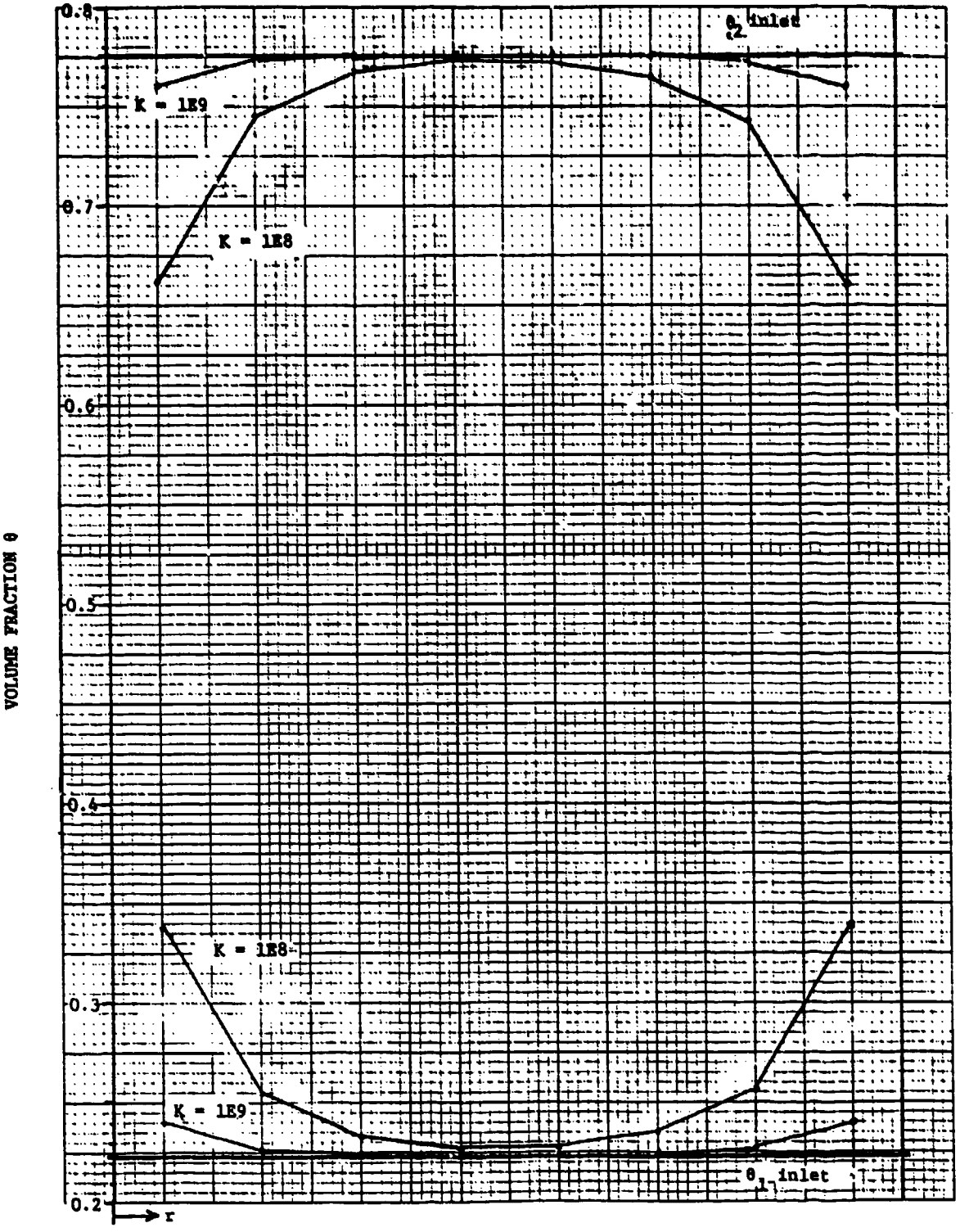

Fig. 4. Volume Fraction Distribution in Fully Developed Annular Flow

the walls. The interfacial drag coefficient (K_{12} = 1.0E8 Pa-s/m^2) is the same as used in the parallel plates case. In addition, two other runs were made with K = 1.0E9 and K = 7.0E10. The results are shown in Fig. 4 where for K greater than 1.0E10 the separation becomes very small.

5. DISCUSSION OF EXPERIMENTAL MEASUREMENTS FOR TRANSPORT PROPERTIES

The following transport properties are needed for the system with a binder and 2 different sizes of particles under consideration so that the set of governing equations with appropriate initial and boundary conditions can be solved.

(1) μ_m needs to be measured vs shear rate and time at the processing temperature.*

(2) D_{2m} and D_{3m} to be measured if possible.

(3) $\underline{f}_2$ and $\underline{f}_3$ shear lift force and gravity force, can be computed (please see Section 5.3).

(4) F_{21} and F_{31} can be estimated (please see Section 5.4).

It is recognized that the transport properties are a function of composition of materials and time history. We recommend that the time history and temperature dependence may be included in some measurements if this can be conveniently done.

5.1 Viscosity Measurements

It is recommended that viscosity be measured with the following compositions, with respect to time and shear rate:

(1) Binder only

(2) Binder + particle 2 (p2) with p2 at 1/3 nominal value.

Binder + p2 with p2 at 2/3 nominal value.

*It is assumed that τ is a function of velocity gradient and mixture viscosity--Non-Newtonian fluid.

Binder + p2 with p2 at full nominal value.

(3) Binder + particle 3 (p3) with p3 at 1/3 nominal value.

Binder + p3 with p3 at 2/3 nominal value.

Binder + p3 with p3 at full nominal value.

(4) Binder + p2 + p3, both p2 and p3 at nominal value.

The viscosity μ of a fluid, in general, exhibits shear rate dependence and can be characterized as follows

$$\mu_m = K \left|\frac{\partial W}{\partial r}\right|^n$$

where K is an empirical constant and $|\partial W/\partial r|$ is the shear rate. The exponent n accounts for various rheological behaviors of the fluid. $n = 0$ for a Newtonian fluid; $n > 0$ for a shear thickening fluid, that is, a viscosity which increases with shear rate; the reverse is the case of $n < 0$, a shear thinning fluid. Depending on the shear rates and the particle size, internal friction or collision, a given fluid may exhibit both ranges of behavior[11]. For the case of a shear thickening fluid ($n = 1$)

$$K = C_\mu \theta_p^2 a^2 \rho_p$$

where C_μ is a constant (= 1 for spheres having elastic collision), θ_p is the volume fraction of particles with radius a[1].

5.2 Diffusivity Measurements

It is recognized that diffusivity cannot be obtained by direct measurement. Therefore, this information may be obtained indirectly through densitometry of particle distributions and photoelasticity of stress measurement of slices from solid propellant specimens. We recommend that these measurements be made at the compositions as outlined in (1) of viscosity measurements. Experimental data is needed, but for a shear thickening fluid ($n = 1$), the particle diffusivity is given by

$$D_{km} = C_d \left(\frac{\rho_m}{\rho_k}\right)\left(\frac{a^2}{\theta_k^3}\right) \left|\frac{\partial W}{\partial r}\right| , \qquad k = 2, 3$$

where C_d is a coefficient of the order of 10[7].

5.3 Field Forces $\underline{f_2}$ and $\underline{f_3}$

These include gravity g, and shear lift forces. The former is negligible for the present case, and the latter has been given analytically for spheres. It will be determined with semi-empiricism in the course of computation by validation from particle density distributions and shear stress distributions in the solid propellant if available. It is given for a spherical particle[3,7] by

$$f_k = C_1[3(6.46)/4\pi](\rho_m/\rho_k) \left[\nu \left(\frac{\Delta W}{a}\right)^2 \left|\frac{\partial W}{\partial r}\right|\right]^{1/2}$$

where W is the velocity outside the boundary layer, $\Delta W = W - W_k$, the velocity difference between the fluid and the particle, a is the particle radius, and $(\partial W/\partial r)$ is the shear rate of the layer. The coefficient C_1 accounts for non-sphericity. Lifting of larger particles by shear motion of small particles will be dealt with in a later report.

5.4 Inverse Relaxation Time

Inverse relaxation times are predictable for spherical particles. For the present application, iteration with empirical coefficients and validation by final particle density distributions can yield semi-empirical modifications for predictive purposes. For particle 2, F_{21} is given by

$$F_{21} = C_F \frac{75\,\theta_2 \bar{\mu}}{2a^2[\rho_2 + (\rho_m/2)]}$$

where C_F is an empirical coefficient, θ_2 is the volume fraction of particles 2, $\bar{\mu}$ is the fluid viscosity, and a is the radius or characteristic dimension of the particle[1].

If all the items in Sections 5.1 and 5.2 can be furnished, they will be most helpful. The order of priority should be

(1) Viscosity measurements.

(2) Densitometry of particle distribution of sliced solid specimens.

(3) Photoelasticity of sliced solid specimens.

The minimum measurement would be flow through a tube and measure the flowrate and pressure drop, from which the viscosity and non-Newtonian parameters can be deduced. We can proceed with results from Item (1) alone. The effort toward achieving a realistic computer program will be facilitated or reduced by having Items (1) and (2), and more so if Item (3) is available.

6. DISCUSSIONS AND CONCLUSIONS

A continuum approach to the modeling of a dense suspension has been taken as opposed to discrete particle tracking. Within the continuum approach, two formulations have been identified: the multifluid model, and the diffusion model. While the multifluid model is more complete, there are more unknown coefficients associated with the model and these coefficients need to be determined. The single velocity diffusion model is computationally more economical and it involves relatively fewer unknown coefficients than the multifluid model. Correspondence between the two models has been pointed out.

A crucial feature needed in the mathematical model is the ability to predict partial component separation from a homogeneous mixture. The only way the single velocity diffusion model can predict partial separation is from the shear lift field force term. The magnitude of this term must be determined experimentally. Due to the current lack of detailed and reliable experimental data, approximations were made for the interaction terms in the multifluid model. Even in the absence of a shear lift field force, the multifluid model can predict partial component separation by having different component velocity boundary conditions at the wall.

In summary, our preliminary investigation of flow modeling during solid propellant processing has yielded the following conclusions:

1. Meaningful prediction of concentration distribution of components can be obtained from computations with a minimal acquisition of transport properties at the initiating phase. These preliminary predictions can be used to guide experiments which are urgently needed to quantify the transport properties and to validate the mathematical models.
2. Currently, the multifluid model and the single velocity diffusion model are viewed as being complementary. While the multifluid model can be used to gain insight into the underlying individual physical mechanisms, the diffusion model gives global phenomenological behavior of the system. The interrelations between the two mathematical models have been clarified. It is anticipated that at a later date, depending on availability of the needed experimental data and understanding of physical mechanisms, we shall select one of the two models as the reference predictive tool.
3. Validation of computed concentrations can be made by sections of solidified models or checked by burning rates for uniformity of pressure.
4. Exploratory calculations have shown the ability of the multifluid model to compute partial separation of components by boundary condition differences. More parametric study can be done to give insight into the sensitivity of the various empirical coefficients.
5. The problem under investigation is important, but very difficult. The preliminary results from the present study lays the foundation for the future work and it appears that useful results can be obtained.

REFERENCES

1. Soo, S. L., Fluid Dynamics of Multiphase Systems, Blaisdell (1967).
2. Bradfield, W. A., Paper No. 35C/69, T.T.C.P. Panels D5 and 03, Joint Meeting, Australia (1969).
3. Saffman, P. G., J. Fluid Mech., Vol. 22, p. 385 (1965).
4. Segré , G., and Silberberg, A., J. Fluid Mech., Vol. 14, pp. 115-136 (1962).
5. Soo, S. L., Appl. Sci. Rev., Vol. 21, p. 68 (1969).
6. Soo, S. L., and Tung, S. K., J. Powder Tech., Vol. 6, p. 283 (1972).
7. Soo, S. L., "Pipe Flow of a Dense Suspension," J. Pipelines, Vol. 6, pp. 193-203 (1987).
8. Jost, W., Diffusion in Solids, Liquids, and Gases, Academic Press, N.Y. (1960).
9. Sha, W. T., Domanus, H. M., Schmitt, R. C., Oras, J. J., and Lin, E.I.H. "COMMIX-1: A Three-Dimensional Transient Single-Phase Component Computer Program for Thermal-Hydraulic Analysis," NUREG/CR-0785, ANL-77-96, Argonne National Laboratory (September 1978).
10. Analytical Thermal Hydraulic Research Program, "COMMIX-1B: A Three-Dimensional Transient Single-Phase Computer Program for Thermal Hydraulic Analysis of Single and Multicomponent Systems. Volume I: Equations and Numerics; Vol. II: User's Manual," NUREG/CR-4348, ANL-85-42, Argonne National Laboratory (September 1985).
11. Brodkey, R., The Phenomena of Fluid Motions, Addison-Wesley (1967).

DISTRIBUTION

	No. of Copies
Commander Naval Weapons Center Code 3272 China Lake, CA 93555-6001	1
Air Force Astronautics Laboratory AFAL/MKPA Edwards Air Force Base, CA 93523-5000	1
Director Ballistic Research Laboratory LABCOM (ATTN: AMDAR-BL) Aberdeen Proving Ground, MD 21005	1
Director U.S. Army Research Office ATTN: DRXRO-IP P.O. Box 12211 Research Triangle Park, NC 27709-2211	1
Naval Surface Weapons Center Code R11 Indian Head, MD 20640	1
Argonne National Laboratory Components Technology Division ATTN: Dr. W. T. Sha 9700 South Cass Avenue Argonne, IL 60439	10
US Army Materiel System Analysis Activity ATTN: AMXSY-MP Aberdeen Proving Ground, MD 21005	1
IIT Research Institute ATTN: GACIAC 10W. 35th Street Chicago, IL 60616	1

Commander
AD (XRC)
ATTN: T. O'Grady 1
Eglin AFB, FL 32542

Aerojet Tactical Systems
ATTN: R. Mironenko 1
P.O. Box 13400
Sacramento, CA 95813

Aerospace Corporation
ATTN: Library Acquisition GP M1-199 1
P.O. Box 92957
Los Angeles, CA 90009

Commander
AFATL
ATTN: CPT Darla M. Roberts 1
Eglin AFB, FL 32542

Commander
AFRPL (DYP)
ATTN: David P. Weaver 1
Edwards AFB, CA 93523

Commander
AFRPL (LK)
Liquid Rocket Division
ATTN: LK, Stop 24 1
Edwards AFB, CA 93523

Commander
AFRPL (MKAS)
ATTN: John H. Clark 1
Edwards AFB, CA 93523

Commander
AFRPL (Tech Lib)
ATTN: Tech Lib 1
Edwards AFB, CA 93523

Commander
AFRPL (TSPR)
ATTN: (TSPR) Stop 24 1
Edwards AFB, CA

Commander
AFSC
ATTN: DLFP 1
Andrews AFB
Washington, DC 20334

Commander
AFWAL (MLTN)
ATTN: Charles S. Anderson 1
Wright-Patterson AFB, OH 45433

Commander
Armament Rsch & Dev Command
ATTN: AMSMC-LC (D), (Dr. Jean-Paul Picard) 1
Dover, NJ 07801

Commander
Armament R&D Command
ATTN: AMSMC-LCA-G(D), (Dr. Anthony J. Beardell) 2
Dover, NJ 07801

Commander
Armament R&D Command
ATTN: AMSMC-SCA-T (D), (Mr. Ludwig Stiefel) 1
BG 455
Dover, NJ 07801

Commander
Armament R&D Comand
Scientific & Tech Div
ATTN: AMSMC-TSS(D) 1
BG 59
Dover, NJ 07801

Director
Army Ballistic Research Labs
ATTN: AMSMC-BLA-S(A), (R. Paul Ryan) 1
Aberdeen Proving Ground, MD 21005

Director
Army Ballistic Research Labs
ATTN: AMSMC-BLI(A), (John M. Hurban) 1
Aberdeen Proving Ground, MD 21005

Director
Army Ballistic Research Labs
ATTN: AMSMC-BLV(A), (Richard Vitali) 1
Aberdeen Proving Ground, MD 21005

Commander
US Army Materiel Command
ATTN: AMCDE-DW 1
5001 Eisenhower Ave
Alexandria, VA 22333

Commander
Army Materiel System Analysis Activity
ATTN: AMXSY-PS-SCTY Spec. 1
Abedeen Proving Ground, MD 21005

Chief
Army Research Office
Information Proc Ofc
ATTN: AMXRO-PP-LIB 1
P.O. Box 12211
Research Triangle Park, NC 27709

Atlantic Research Corp.
ATTN: Technical Info. Ctr 2
7511 Wellington Rd.
Gainesville, VA 22065

California Institute of Technology
Jet Propulsion Laboratory
ATTN: Lib. Acqs/Standing Orders 1
Floyd A. Anderson 1
4800 Oak Grove Drive
Pasadena, CA 91103

Administrator
Defense Technical Information Center
ATTN: DTIC-DDA 2
Cameron Station BG 5
Alexandria, VA 22314

Commander
ESMC(PM/STINFO)
ATTN: L. M. Adams 1
Patrick AFB, FL 32925

FMC Corp., Northern Ord. Div
ATTN: Library, (E. Schultz) 1
4800 East River Rd
Minneapolis, MN 55421

Ford Aerospace & Comm. Corp.
Aeronutronic Division
ATTN: Tech Inf. Svc/DDC Acqs. 1
Ford & Jamobree Roads
Newport Beach, CA 92663

Commander
FTD(TQTA)
ATTN: Arnold Crowder 1
Wright-Patterson AFB, OH 45433

Commander
FTD(SDBP)
ATTN: SDBP 1
Wright-Patterson AFG, OH 45433

Gould Defense Sys. Inc.
Ocean Systems Div.
ATTN: Info. Ctr, Dept. 749 PLT 2
R. J. Rittenhouse 1
18901 Euclid Ave.
Cleveland, OH 44117

Hercules Inc.
Aerospace Div, Allegany Ballistics Lab.
ATTN: Library 1
P.O. Box 210
Cumberland, MD 21502

Hercules, Inc.
Bacchus Works
ATTN: 100-H-2-LIB (W. G. Young) 1
P.O. Box 98
Magna, UT 84044

Hercules, Inc.
ATTN: Pub. Coord (D. A. Browne) 1
P.O. Box 548
McGregor, TX 76657

Hughes Aircraft Co.
Electro Optical & Data Sys. Group
ATTN: Tech Doc Ctr, BG E1E110)
B. W. Campbell 1
P.O. Box 902
El Segundo, CA 90245

Johns Hopkins University
Applied Physics Lab, Chem. Prop. Inf. Agy.
ATTN: Code ML, R. D. Brown 2
Johns Hopkins Road
Laurel, MD 20707

LTV Aerospace & Def. Co.
ATTN LIB 2-58010 1
P.O. Box 225907
Dallas, TX 75265

Marquardt Company
ATTN: LIB 1
P.O. Box 2013
Van Nuys, CA 91409

Martin Marietta Corp.
ATTN: MP-30-TIC 1
P.O. Box 5837
Orlando, FL 32855

National Aeronautics & Space Admin.
George C. Marshall Space Flt Ctr.
ATTN: AS24L 1
Marshall Space Flight Center, AL 35812

National Aeronautics & Space Admin.
George C. Marshall Space Flight Center
ATTN: EP-25, Mr. John Q., Miller 1
Marshall Space Flight Center, AL 35812

National Aeronautics & Space Admin
Langley Research Center
ATTN: MS-185 Tech. Lib. 1
Hampton, VA 23665

National Aeronautics & Space Admin.
Lewis Research Center
ATTN: Lib(D. Morris) 1
21000 Brookpark Rd.
Cleveland, OH 44135

National Aeronautics & Space Admin.
Lewis Research Center
ATTN: MS-501-5, D. A. Petrash 1
21000 Brookpark Rd.
Cleveland, OH 44135

National Aeronautics & Space Admin.
Lyndon B. Johnson Space Center
ATTN: JM2/Tech. Lib. 1
Houston, TX 77058

National Aeronautics & Space Admin.
Scientific Technical Info. Fac.
ATTN: Accessioning Dept. 1
P.O. Box 8757
Baltimore Washington Intl Airport, MD 21240

Commander
Naval Air Dev. Ctr.
ATTN: Code 8131 1
Warminster, PA 18974

Commander
Naval Air Sys. Comd.
ATTN: NAIR-00D4-Tech Lib. 1
Washington, DC 20361

Commander
Naval Air Sys Comd
ATTN: NAIR-320G, Mr. Bertram P. Sobers 1
Washington, DC 20361

Commander Officer
Naval Intel Spt Ctr
Information Svc Div
ATTN: Doc Lib 1
4301 Suitland Rd.
Washington, DC 20390

Commanding Officer
Naval Ord Sta-Indian Head
ATTN: Tech Lib, Code 4243C, Henrietta Gross 1
Indian Head, MD 20640

Superintendent
Naval Postgraduate Sch.
ATTN: Code 1424-Libs Dir 1
Monterey, CA 93943

Chief Naval Research
ATTN: Dr. Richard S. Miller, Code 432 1
Arlington, VA 22217

Chief
Naval Research
ATTN: R. Junker, Code 412 1
Arlington, VA 22217

Commanding Officer
Naval Research Lab
ATTN: Code 6100 1
Washington, DC 20375

Director
Naval Arsearch West Pasadena
ATTN: R. J. Marcus 1
1030 E Green St
Pasadena, CA 91106

Commander
Naval Sea Sys Comd
ATTN: SEA-09B312, Tech Lib 1
Natl Ctr BG 3
Washington, DC 20362

Commander
Naval Sea Sys Comd
ATTN: Mr. Elgin Werback, SEA-62Z31B 1
Natl Ctr BG 3
Washington, DC 20362

Commander
Naval Surface Wpns Ctr
ATTN: Acquisitions, Code E431 1
Dahlgren, VA 22448

Commander
Naval Surface Wpns Ctr
ATTN: Code E432, S. Happel, Room 1-321 2
Silver Spring, MD 20910

Commanding Officer
Naval Underwater Sys Ctr
ATTN: Tech Lib 021312 1
Newport, RI 02840

Commander
Naval Weapon Center
ATTN: Code 343 2
China Lake, Ca 93555

Director
Navy Strat Sys Proj Ofc
ATTN: Tech Lib Br Hd 1
Washington, DC 20376

Commander
Ogden ALC (MANPA)
ATTN: Mr. Anthony J. Inverso 1
BG 1941
Hill AFB, UT 84056

Commander
Radford Army Ammo Plant
ATTN: SMCRA-QA 1
Radford, VA 24141

Rockwell Int'l Corp.
Rocketdyne Div
ATTN: Tech Info Ctr 1
6633 Canoga Ave
Canoga Park, CA 91304

Rohm & Haas Co.
ATTN: Scty Off, (Dr. H. M. Shuey)
723-A Arcadia Circle
Huntsville, AL 35801

Commander
SAALC (SFTT)
ATTN: W. E. Vandeventer 1
Kelly AFB, TX 78241

SRI Int'l Document Ctr
ATTN: Classified Doc Svc, (Dr. Clifford D. Bedford) 1
333 Ravenswood Ave
Menlo Park, CA 94025

Talley Industries
ATTN: Eng. Tech Lib, (Kim St. Clair) 1
P.O. Box 849
Mesa, AZ 85201

Teledyne Ryan Aeronautical
ATTN: Tech Info Svcs (W. E. Ebner) 1
2701 Harbor Drive
San Diego, CA 92101

Thiokol Chem Corp
Wasatch Div
ATTN: Tech Lib (J. E. Hansen) 2
Brigham City, UT 84302

Thiokol Corp.
ATTN: Scty Off, (D. J. McDaniel) 1
P.O. Box 241
Elkton, MD 21921

Thiokol Corp.
ATTN: Tech Lib (H. H. Sellers) 1
Huntsville, AL 35807

TRW Inc.
Electronics & Defense Sector
ATTN: Tech Inf Ctr, Doc Svcs for S/1930 2
One Space Park
Redondo Beach, CA 90278

TRW Inc.
Electronics & Defense Sector
ATTN: Tech Inf Ctr, Doc Svcs
for R. C. Reeve, San Bernardino 1
One Space Park
Redondo Beach, CA 90278

USDRE (PCA)
ATTN: OUSDRE&E (R&AT/MST), (Dr. Robert J. Heaston) 1
The Pentagon, Room 3D1089
Washington, DC 20301

United Technologies Corp
Chemical Systems Div
ATTN: Tech Lib 1
P.O. Box 358
Sunnyvale, CA 94088

United Technologies Corp.
Research Center
ATTN: Acq Lib (M. E. Donelly) 1
400 Main Street
East Hartford, CT 06108

Commander
White Sands Missile Range
ATTN: Tech Lib 1
White Sands Missile Range, NM 88002

AMSMI-RD, Dr. McCorkle	1
Dr. Rhoades	1
AMSMI-RD-RE, Dr. Hartman	1
Dr. Bennett	1
AMSMI-RD-PR, Dr. Stephens	1
Dr. Wharton	1
AMSMI-RD-PR-T, Dr. Alley	1
Mr. Allen	1
AMSMI-RD-PR-P, Mr. Schultz	1
AMSMI-RD-PR-M, Mr. Ifshin	1
AMSMI-RD-PR-E, Mr. Maykut	5
AMSMI-RD-CS-R	15
AMSMI-RD-CS-T	1
AMSMI-GC-IP, Mr. Bush	1

*U.S. GOVERNMENT PRINTING OFFICE: 1988-530-081/80110 Region 4.